Diamond & Related Materials 135 (2023) 109879

Contents lists available at ScienceDirect

Diamond & Related Materials

journal homepage: www.elsevier.com/locate/diamond

Time-of-flight photoconductivity investigation of high charge carrier mobility in $Ti_3C_2T_x$ MXenes thin-film

Jurij Urbančič [a], Erika Tomsič [a], Manisha Chhikara [a], Nadiia Pastukhova [a], Vadym Tkachuk [a], Alexander Dixon [a], Andraž Mavrič [b], Payam Hashemi [c,d], Davood Sabaghi [c], Ali Shaygan Nia [c,d], Gvido Bratina [a], Egon Pavlica [a,*]

[a] Laboratory of Organic Matter Physics, University of Nova Gorica, Vipavska 13, Nova Gorica SI-5000, Slovenia
[b] Materials Research Laboratory, University of Nova Gorica, Vipavska 13, Nova Gorica SI-5000, Slovenia
[c] Center for Advancing Electronics Dresden (cfaed) and Department of Chemistry and Food Chemistry, Technische Universität Dresden, Mommsenstrasse 4, Dresden 01069, Germany
[d] Department of Synthetic Materials and Functional Devices, Max-Planck-Institut für Mikrostrukturphysik, Weinberg 2, 06120 Halle (Saale), Germany

ARTICLE INFO

Keywords:
Charge transport in multilayered network of flakes
Time-of-flight photoconductivity
MXene exfoliation
High-mobility solution-cast thin-film
Semiconducting mxene

ABSTRACT

Charge transport through a randomly oriented multilayered network of two-dimensional (2D) $Ti_3C_2T_x$ (where T_x is the surface termination and corresponds to O, OH and F) was studied using time-of-flight photoconductivity (TOFP) method, which is highly sensitive to the distribution of charge carrier velocities. We prepared samples comprising $Ti_3C_2T_x$ with thickness of 12 nm or 6-monolayers. MXene flakes of size up to 16 μm were randomly deposited on the surface by spin-coating from water solution. Using TOFP, we have measured electron mobility that reached values up to 279 cm^2/Vs and increase with electric-field in a Poole-Frenkel manner. These values are approximately 50 times higher than previously reported field-effect mobility. Interestingly, our zero-electric-field extrapolate approaches electron mobility measured using terahertz absorption method, which represents intra-flake transport. Our data suggest that macroscopic charge transport is governed by two distinct mechanisms. The high mobility values are characteristic for the intra-flake charge transport via the manifold of delocalized states. On the other hand, the observed Poole-Frenkel dependence of charge carrier mobility on the electric field is typical for the disordered materials and suggest the existence of an important contribution of inter-flake hopping to the overall charge transport.

1. Introduction

The field of 2D materials was triggered by the introduction of graphene in 2004 [1]. Since then, many different 2D materials were synthesized and intensively studied, mainly due to their thickness of a single layer of atoms and their unique low-dimensionality driven electronic properties that sets them apart from the bulk (3D) materials. Electron confinement in 2D is frequently characterized by reduced nuclear scattering and, consequently high electron mobility. For example, in graphene values as high as 20×10^4 cm^2/Vs were reported [2]. However, its semi-metallic character precludes its use in high-speed switching applications. Opening of the electronic energy gap has been observed in graphene nanoribbons (E_g = 150 meV), but it is coupled to drastic reduction of mobility ($\mu = 200$ cm^2/Vs) [3]. On the other hand, selected 2D transition metal dichalcogenides (TMDs) exhibit a direct electronic energy gap that would allow their use in switching applications, but their use is limited due to relatively low charge carrier mobility, which in MoS_2 amounts to values exceeding 150 cm^2/Vs [4–6].

MXenes represent a novel family of 2D transition-metal carbides, nitrides or carbonitrides. After their first experimental realization in 2011 [7], more than 70 species of MXenes were already synthesized and many more were theoretically predicted [8–10]. MXenes are produced from a layered metallic ceramic $M_{n+1}AX_n$ (n = 1 to 3) phase, where M represents the transition metal, A is a III or IV A-group element and X is carbon and/or nitrogen. Selective etching of the A atoms, usually using fluoride-based acids or salts leads to the formation of $M_{n+1}X_nT_x$, where T_x is the surface termination group such as F, O and OH that depends on synthesis and delamination procedure [11] and renders the surface of the flakes hydrophilic [12]. These properties make MXenes promising candidates for numerous applications such as energy storage in lithium-

* Corresponding author.
E-mail address: egon.pavlica@ung.si (E. Pavlica).

https://doi.org/10.1016/j.diamond.2023.109879
Received 28 November 2022; Received in revised form 23 January 2023; Accepted 19 March 2023
Available online 23 March 2023

ion batteries [13–15], sensors, electronic devices, catalysts, conductive reinforcement additives to polymers [16]. Most pure MXenes are metallic (with some exceptions being semiconductors - like Ti_2CO_2) [7,17,18] due to relatively high density of states (DOSs) near the Fermi level [19]. Moreover, with proper functionalization, metallic MXenes can be transformed to semiconducting [20]. Mechanical strain has also been used to tune the direct band gap in some MXenes [21].

Charge transport in MXenes has also been a subject of several recent theoretical [22,23] and experimental studies [23]. We have selected to characterize charge transport properties of $Ti_3C_2T_x$. It exhibits a breakdown current density in the order of 10^8 A/cm^2 and electric conductivity above 10^4 S/cm [24]. We embarked onto a detailed study of charge carrier transport in this material with the emphasis on the elucidation of the role of interfaces between $Ti_3C_2T_x$ flakes. Charge carrier transport in the plane of the MXene flakes is known to proceed via extended states [23] and is characterized by single-flake mobilities above 10^3 cm^2/Vs [25]. Less clear is charge transport in thin layers comprising an ensemble of 2D flakes in close proximity to each other. To elucidate this point we have employed time-dependent photoconductivity measurements in coplanar-electrode geometry [26], which yields information on the charge transport through the whole layer and not only at the interface with gate-dielectric, which is the case with thin-film transistors (TFTs). Our results show that charge carrier mobility exceeds values of 100 cm^2/Vs in continuous film of overlapping $Ti_3C_2T_x$ flakes. We explain these results in terms of combined charge transport through extended energy states residing on the flakes and through the localized states at the inter-flake interfaces.

2. Experimental section

We have synthesized $Ti_3C_2T_x$ by etching Ti_3AlC_2 using hydrofluoric acid. A detailed procedure is reported in Supplementary Information. The MXene samples for the TOFP measurement were prepared on high quality quartz glass substrates that were cleaned in an ultrasonic bath of acetone, followed by isopropanol and rinsed with distilled water. These substrates were subsequently surface-treated with nitrogen plasma for 10 min and exhibited rms surface roughness lower than 0.3 nm (see Fig. S1 in Supplementary Information). Immediately after plasma treatment, the substrates were transferred into a nitrogen-filled glovebox with H_2O and O_2 levels below 1 ppm. The 10 mg/ml solution of MXene in H_2O was spin-coated on top of plasma-treated substrate at 5000 rpm for 1 min. Such high rpm is required in order to obtain homogeneous coating due to the viscoelastic property of MXenes [27]. Since high temperatures [28] (along with oxygen in the presence of water [29]) accelerate the decay of MXenes, the samples were subsequently dried in high vacuum (2×10^{-7} mbar) at room temperature for 3 days. Coplanar gold electrodes separated by 250 μm were deposited onto the MXene layer through a shadow mask by high-vacuum electron-beam evaporation. The space between electrodes is referred to as channel in the forthcoming text. To analyze the morphology and structure of the prepared MXene layer on quartz, we employed grazing incidence x-ray diffraction (XRD), scanning electron microscopy (SEM) and atomic force microscopy (AFM).

Charge carrier mobility in pure MXene layers was characterized using a time-of-flight photoconductivity (TOFP) method which is explained more in detail in Ref. [26]. A constant bias V_b was applied between the two gold electrodes. In what follows we will refer to the "biased electrode" the one that is at higher electrical potential than the opposite electrode, which we will refer to as "collecting electrode". We varied the bias in the range of +150 V to −150 V. Charge carriers were excited by laser pulses provided by an optical parametric amplifier with a pulse duration of 3 ns and a repetition rate of 3 Hz. To ensure a spatial localization of the photoexcited carriers, the laser beam was focused into a line near the biased electrode through the use of a cylindrical lens. The width of the laser line was 10 ± 2 μm. The photoexcited charge carriers drifted in the electric field present within the MXene layer, and the resulting current $I(t)$ was fed into a 4 GHz current amplifier and subsequently measured as a voltage drop over an input resistor by 2.5 GHz digitizing oscilloscope. From the line shape of I(t) we have determined the charge carrier transit time needed to travel the interelectrode space and from transit time the charge carrier mobility was determined.

3. Results and discussion

Recently it has been shown that charge transport along a MXene flake differs in a profound way from the transport between the flakes. Band-like transport is characteristic for intra-flake charge carrier transport. Between the flakes instead, thermally-activated charge carrier hopping was found to be the predominant mechanism [23]. Since the dimensions of devices based on MXene flakes exceed several flakes, the latter transport mode ultimately limits the charge current that can be transported in a network of MXene flakes that may be overlapping or just touching. While the structure of an individual flake is crucial for the band-like transport, the morphology, i.e., mutual flake alignment within the MXene layer comprising many flakes determines the inter-flake transport.

Relatively uniform orientation of the MXene flakes is confirmed by the SEM using secondary electron emission at 15 kV (Fig. 1a). A network of MXene flake edges is seen as elongated features of a lighter tone. By resolving the edges of flakes on the surface, we were able to calculate the flakes' size, which we report as a square root of their area. Quite significant number of flakes exhibit sizes in the range between 6 μm and 16 μm (see Fig. S4). XRD spectrum (Fig. 1b) exhibits a single sharp peak at $2\theta = 7.0°$, corresponding to the reflection from (002) plane of the flakes with interplanar crystal spacing of 12.46 Å, consistent with already reported diffraction peaks of MXenes [30,31]. The absence of any additional peaks confirms an absence of crystalline impurities, and phases with different interlayer spacing, indicating a complete exfoliation of MXenes from the original MAX phase. It also indicates that the vast majority of the flakes is oriented with the (002) plane parallel to the substrate. Sample thickness of 12 nm was estimated by scratching the edge with a plastic tip and measuring the morphology profile with AFM (see Fig. S2 in Supplementary Information).

These combined investigations of thin MXene layers on quartz therefore confirm high degree of uniformity of the alignment of the flakes and their complete exfoliation. They are oriented parallel on the substrate surface and form at most 6 layers. Due to relatively high density of grain boundaries we expect that inter-flake hopping will be of considerable importance in determining the charge carrier transport across the MXene layer. In addition, imperfect mutual alignment of the flakes, inevitably leads to the emergence of traps that immobilize charge carriers and further decrease their mobility.

To characterize charge carrier transport in MXene layers we have selected to use TOFP because (i) it provides statistical distribution of charge carrier velocities, which is desirable for unarranged stacking of flakes and (ii) it probes charge transport through the whole layer, and not only at the interface with the gate dielectric, which is the case for, e.g. thin film transistors [26]. Of particular importance for TOFP experiments is the selection of the wavelength of the charge-carrier excitation light. We have already demonstrated that different charge transport channels can be accessed in blended layers of graphene and perylene derivatives (PDIF-CN2) [32]. By changing the excitation wavelength from maximum absorption in PDIF-CN2 to the UV region of increased absorption in graphene, we have detected almost two orders of magnitude shorter transit times. We interpreted this phenomenon with the ability of electrons excited by UV light into high-energy states of graphene to travel through the blended layer with minimal nuclear scattering.

We first focus on the optical absorption in $Ti_3C_2T_x$. Previous reports suggest that optical absorption spectra of $Ti_3C_2T_x$ depends on the surface termination [33,34]. O- and F-terminated species exhibit considerably lower absorption for the photon energies below 3 eV. Common to all is a

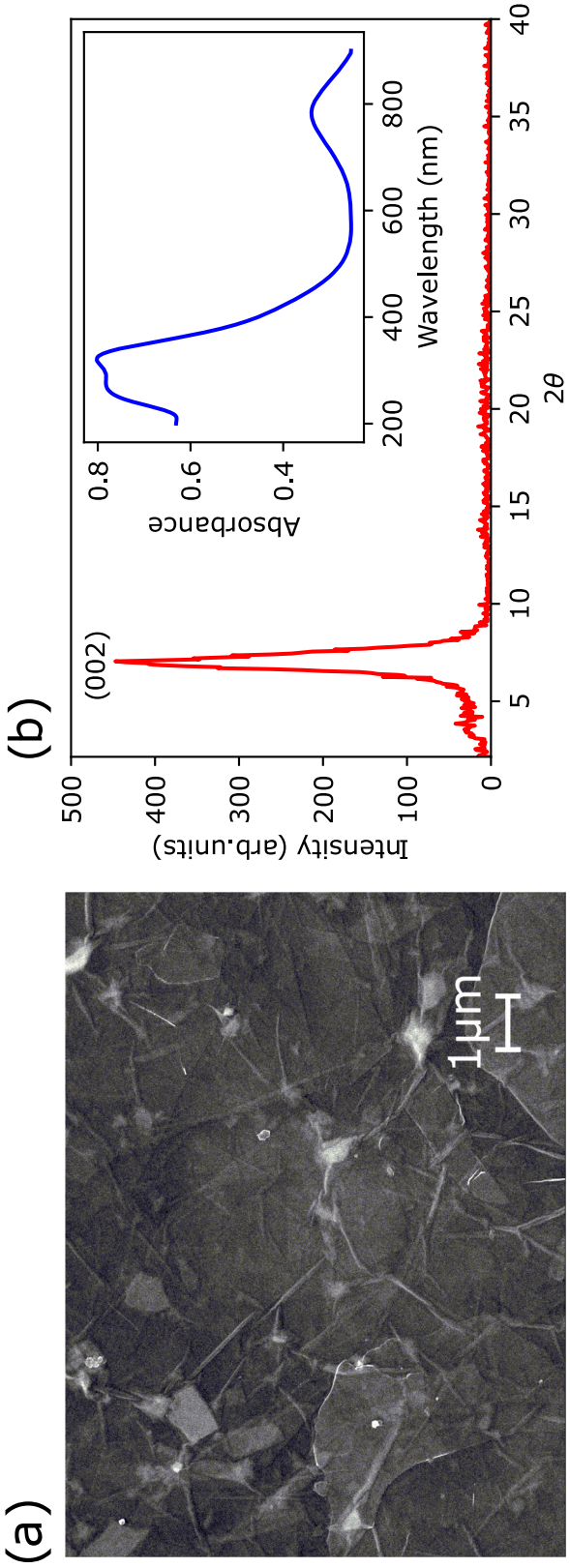

Fig. 1. a) SEM image of the surface of thin layer of $Ti_3C_2T_x$ deposited on quartz substrate by spin-coating. The image was obtained by secondary electron emission at electron accelerating voltage of 15 kV. A network of elongated structures of lighter tones represents folds and boundaries of individual flakes. b) Grazing incidence X-ray diffraction spectrum of a thin layer of $Ti_2C_3T_x$ deposited on a quartz substrate by spin-coating. The peak labelled (002) appears at $2\theta = 7.0^\circ$ and corresponds to a diffraction from the{002} planes of the flakes. Inset: UV-VIS absorption spectrum of $Ti_3C_2T_x$ in water solution. Absorption peaks at 320 nm and 270 nm are due to the inter-band transitions. The additional peak around 780 nm is due to the localized surface plasmon resonance.

relatively high absorption of photons with energies beyond 4 eV [33,35], where intra-band transitions dominate, as opposed to plasmonic losses that dominate low-energy part of the spectrum [36]. For metallic-like MXenes such as $Ti_3C_2T_x$ inter-band transitions result in a distribution of hot electrons [37], which in the external electric field give rise to a measurable photocurrent. UV-VIS absorption spectra of $Ti_3C_2T_x$ in a water solution with concentration lower than 0.01 mg/ml is shown in the inset of Fig. 1b. Two prominent peaks at 320 nm and 270 nm (due to inter-band transitions [38]) are visible in addition to a much lower one at 780 nm (belonging to localized surface plasmon resonance [39]). To maximize the photoabsorption and consequently the photoelectron yield from the $Ti_3C_2T_x$ layer we have set the wavelength of the excitation light to 270 nm (4.59 eV) – with the photon energy slightly above of the highest absorption peak. Note that this photon energy is lower than the workfunction of Au electrodes (5.1 eV), so that the eventual electrons resulting from the photoelectric effect and the associated photoelectron current is effectively quenched.

Using excitation of 270 nm, we varied the bias between +150 V and − 150 V. For positive polarities of V_b, the magnitude of the photocurrent was below the noise level indicating that the majority of the excited charge carriers are electrons (see Fig. S3). Fig. 2a shows $I(t)$ in a double logarithmic plot measured at V_b ranging from −50 V to −150 V. Some of the photogenerated charge carriers may collide with trap states (either on the surface or in the bulk) and become trapped for longer times than the duration of the measurement and do not participate in the charge transport anymore, while others are released soon after the trapping. This stochastic trapping typically results in a monotonically decreasing $I(t)$, absent of any region of constant current [26]. As the charge carriers reach the collecting electrode the $I(t)$ line shape exhibits a distinct change of slope [40]. This point marks the t_{tr}. Rapid change of slope, as we have observed, is a direct experimental evidence of a coherent arrival of a part of photoexcited charge carriers, which exhibit the fastest drift velocities. Several methods to determine the t_{tr} from the $I(t)$ line shape have been proposed [26]. Here we devised an *I(t)* model, which is based on a method put forth by Scher and Montroll that is based on approximating the line shape before and after the change of slope by a linear asymptotic function [41]. The t_{tr} is located at the intersection of the two lines [41]. In addition to two asymptotes, our model empirically resolves the transition region in-between, where *I(t)* changes its slope:

$$I(t) = I_0 \bullet \left(\frac{t}{t_{tr}}\right)^{\alpha-1} \bullet \left(1 + \left(\frac{t}{t_{tr}}\right)^{\gamma}\right)^{\frac{-\beta}{\gamma}} \quad (1)$$

where α and β determine *I(t)* slope before and after t_{tr}. Both, α and β are unitless parameters connected to charge trapping and de-trapping dynamics. Value of α is restricted between 0 and 1 and was formerly introduced as dispersion parameter [42]. While γ represents the width of the transition region. It quantifies the distribution of transit times of the subgroup of those charge carriers, which induced the change of *I(t)* slope. Using Eq. (1) to describe I(t) in Fig. 2b, we obtained values of α, β, γ (Fig. 2c) and t_{tr} (Fig. 2b). From the values of t_{tr}, V_b and channel length (L) the time-of-flight charge carrier mobility (μ) was calculated (Fig. 2b) using relation $\mu = \frac{\pi^2}{8} L^2 / V_b t_{tr}$, which stems from the assumption of a charge carrier drifting with a constant mobility in a position-dependent electric field formed between coplanar electrodes when an external bias voltage is applied [26].

The resulting values t_{tr} and μ as a function of square-root of the applied electric field (with the electric field being approximated as $E = V_b/L$) are summarized in Fig. 2b. We can observe that t_{tr} scales inversely with applied voltage V_b. Stronger electric field caused by larger values of V_b results in faster charge carrier transport across the $Ti_3C_2T_x$ layer [43]. An examination reveals a mobility dependence on the applied electric field, going from 146 cm^2/Vs at −50 V to 279 cm^2/Vs at −150 V. The dependence on the electric field is a typical characteristic of the charge transport in disordered systems, while relatively high charge mobility,

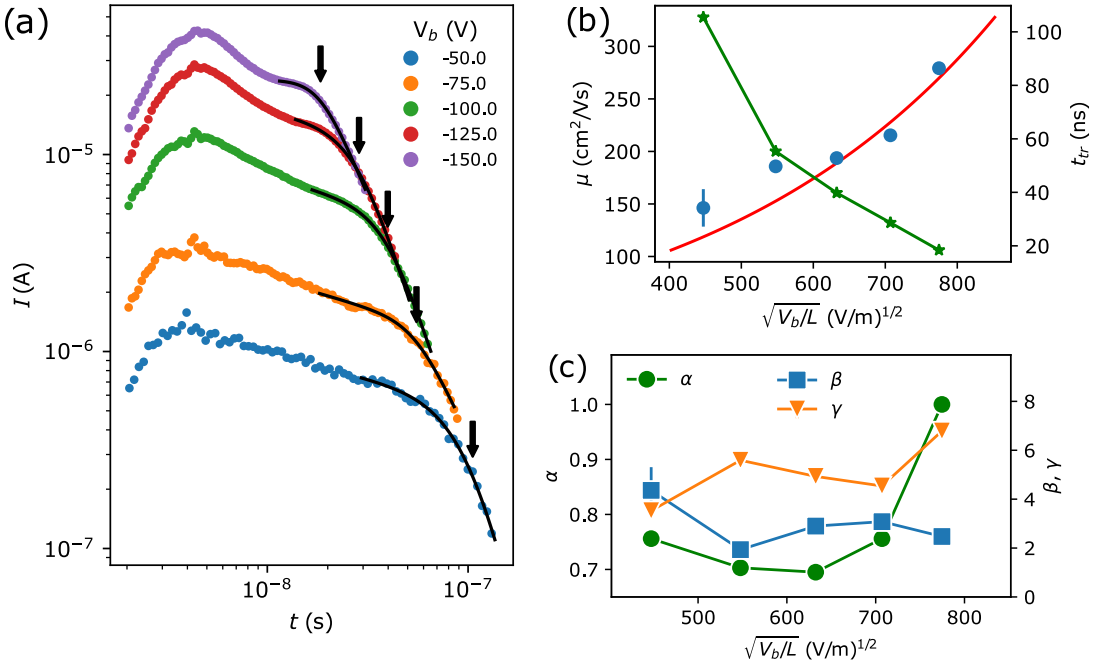

Fig. 2. a) Time-dependent photocurrent ($I(t)$) in a double-logarithmic scale, measured by exciting a 12 nm thick $Ti_3C_2T_x$ layer on quartz with 3 ns light pulses having a wavelength of 270 nm. The separation of two coplanar electrodes was 250 μm. Different colors of the symbols represent measurements performed at different values of interelectrode bias (V_b). Solid lines represent $I(t)$ the model given by Eq.(1). Arrows mark transit time t_{tr}. b) Transit times (green stars) and electron mobility (blue circles) as a function of the square-root of the applied electric field. The red solid line represents the fit to the Eq.(2). c) Parameters of Eq.(1) as a function of square-root of applied electric field corresponding to $I(t)$ presented by solid lines in (a) (See text for details.)

similar to the values of crystalline systems, suggest that the charge transport in our MXene layers is of mixed type. This is consistent with recently presented studies of charge transport in $Ti_3C_2T_x$ and $Nb_4C_3T_x$ MXenes [23], where the dual character of charge transport was reported. Band-like transport is characteristic for intra-flake charge carrier transport with mobilities exceeding 10^3 cm^2/Vs [25]. Between the flakes instead, thermally-activated charge carrier hopping was found to be the predominant mechanism [44]. As confirmed from the morphology images, c.f. Fig. 1, our layers comprise $Ti_3C_2T_x$ flakes that are in close proximity to each other, indicating a percolative conduction path through the whole layers. The interface between the flakes is therefore likely to be characterized by the presence of states residing at the flake edges, exhibiting thereby a relatively high degree of localization. This in turn is responsible for trapping electrons and thereby decreasing the macroscopic mobility across the channel. t_{tr} is thus dependent on the time the carriers remain in a localized state. Higher external electric fields in turn suppress the potential barrier between these localized states, and reduces the release time [45]. This results in the mobility being positively proportional to the applied electric field. To explain the dependence of mobility on the electric field in materials with localized states, the Poole-Frenkel effect [46–48] is employed, expressed by

$$\mu(E) = \mu_0 e^{\beta\sqrt{E}}. \tag{2}$$

where μ_0 is the zero-field mobility, β is the Poole-Frenkel coefficient and E is the applied electric field. The Poole-Frenkel coefficient is related to the hopping distance [49] and the zero-field mobility is the intrinsic charge carrier mobility without the external electric field reducing the hopping barrier [50]. By fitting the data from Fig. 2b with this model, we estimate the μ_0 to be 38 ± 15 cm^2/Vs and β as (2.5 ± 0.6) × 10^{-2} (cm/V)$^{1/2}$.

The observed values of mobility are close to the values observed in the intra-flake charge carrier transport of other MXenes ($TiCO_2$, Hf_2CO_2 and Zr_2CO_2), where values with mobilities exceeding 10^3 cm^2/Vs [25]. Our results agree well with the findings of Zheng et al. [23]. They interpreted the results of their charge transport measurements based on ultrafast terahertz spectroscopy and static conductivity in terms of large optical polarons, which effectively screen defect's potential. Therefore, polaronic intra-flake transport is protected from scattering and trapping although our layers are deposited from solution and contain high density of structural defects. Meaning that the defects does not trap charge carriers during intra-flake transport. By knowing high defect tolerance of charge mobility in a single MXene flake, we can consider inter-flake transport-related effects. To our knowledge, charge mobility in polycrystalline layers is orders of magnitude lower compared to single-crystal mobility [40] [51]. Related to this, Kinetic Monte Carlo (KMC) simulations of charge transport in polycrystalline layers yield important step forward. Meier et al. [52] represented KMC simulation of charge transport in polycrystalline layers, studying the role of grain boundaries on the effective charge mobility. They report that thickness and the electronic energy levels of grain boundaries control the alignment of Fermi level at the interface between crystalline and amorphous boundary region. In the case, when grain boundaries are wide and of lower energy, charge carriers prefer to accumulate into these amorphous domains, reducing the effective charge mobility by several orders of magnitude compared to the charge mobility of crystalline domains. In contrast, when grain boundaries represent a small fraction of the layer and when their energy levels are relatively close to levels in crystalline domains, the delocalized transport dominate in crystalline regions, while electronic states in grain boundaries represent minority trapping sites. By reducing the boundary thickness, they found, the tunneling occurs through grain boundaries between neighboring crystalline domains. Their most important KMC simulation result is that the field-effect mobility of a polycrystalline layers reaches in a best case up to 10 % of the charge mobility of the crystalline domains [52]. TOFP probe charge transport throughout the layer and is not sensitive only to the interface of gate dielectric, as is the case of the field-effect mobility measurements [53]. Thus, the transport properties involve paths in the entire layer and not only in the region near the gate-dielectric interface. Kovtun et al. [54] were studying the charge transport through multi-layered randomly stacked films of reduced graphene oxide flakes. They

realized that the flake-to-flake interfaces do not limit the charge transport, but instead, these interfaces represent an advantageous bypass in the percolative pathway of the charge carrier. Therefore, the drift velocity of charge carriers through a two-dimensional multilayered network of randomly oriented flakes is in principle able to retain the values of a single crystalline domain. Based on their findings, we suggest that the charge mobility of the fastest carriers, which we measured using TOFP method, reflects the charge mobility of the intra-flake domain.

The high values of mobility observed can be therefore attributed to (i) the layer fabrication and (ii) the synthesis process that is able to produce high quality and stable MXene flakes. Related to the later, these flakes also exhibit large lateral size that results in a conductive path with fewer hopping processes. Related to the layer fabrication, when considering the mobility of a thin-film made of 2D materials, the surface morphology must be taken into account [55,56]. Jammed and obliquely aligned flakes result in a weak overlap between the plane of the flakes. This leads to high parasitic resistance at the flakes interface and a reduction in macroscopic mobility. Thus, the improved exfoliation method and the deposition on the substrate results in a good inter-flake connectivity that enhances the inter-flake charge transfer. This reflects in the measured charge mobility, which is substantially higher than previously published results. However it was shown that using different synthesis methods and processing routes for $Ti_3C_2T_x$ can yield significantly different transport properties [57]. Also, we have taken a special care to avoid oxidation of the $Ti_3C_2T_x$ edges, which irreversibly damages the flakes and reduces charge carrier mobility. Several previous experimental studies of $Ti_3C_2T_x$ show varying carrier mobilities of 6 cm^2/Vs (field-effect electron mobility [24]), 0.9 cm^2/Vs (Hall effect measurements [58]), and 34 cm^2/Vs (THz spectroscopy [59]). Although these mobilities are obtained using different experimental methods, we note that the charge carrier mobility in $Ti_3C_2T_x$ is extremely dependent on the degree of edge oxidation, surface termination and chemical surrounding of e.g. surfactants and exfoliation agents.

4. Conclusion

We fabricated layers comprising multi-layered, randomly oriented $Ti_3C_2T_x$ MXene flakes and characterized charge carrier transport in them. The results of time-of-flight photoconductivity measurements confirm electron transport with mobilities up to 279 cm^2/Vs, which is substantially higher than previously reported field-effect mobility, which was below 10 cm^2/Vs. The extrapolated zero-field mobility of 38 $\pm$ 15 cm^2/Vs reaches values measured in single $Ti_3C_2T_x$ MXene flakes (34 cm^2/Vs). We suggest that this is a consequence of precise MXene exfoliation and efficient deposition process. The exfoliation yielded flakes with the largest dimensions on the order of several microns. The deposition of the layers resulted in up to 6-layer-thick film of interconnected randomly oriented flakes. We demonstrate that the transport through such randomly connected percolation network can be characterized as charge transport through crystalline flakes, perturbed by trapping in the localized states, residing at the interfaces between the flakes. The former process results in high charge mobility, the latter results in a low charge carrier mobility. This duality is likely to be responsible for relatively high values of TOFP-measured charge carrier mobility. These results also suggest that charge trapping at the dielectric interface becomes less important when the charge carriers are transported through several pristine MXene layers above and away from the dielectric interface as in our TOFP experiments. This results in overall higher observed charge carrier mobility. On the other side, the charge carrier mobility exhibits positive dependence on the electric field of the Poole-Frenkel type, which is typical for disordered material. This behavior seems to be pertinent to a multilayered network of randomly distributed flakes with an interfacial electronic structure, which does not suppress the charge transport, but it represents a bypass to improved charge carrier transport.

CRediT authorship contribution statement

Jurij Urbančič: Conceptualization, Validation, Formal analysis, Investigation, Writing – original draft, Visualization. **Erika Tomsič:** Investigation. **Manisha Chhikara:** Investigation, Resources. **Nadiia Pastukhova:** Investigation. **Vadym Tkachuk:** Investigation. **Alexander Dixon:** Conceptualization, Validation, Formal analysis, Investigation. **Andraž Mavrič:** Investigation. **Payam Hashemi:** Investigation, Resources, Writing – original draft. **Davood Sabaghi:** Resources. **Ali Shaygan Nia:** Conceptualization, Methodology, Writing – review & editing, Supervision. **Gvido Bratina:** Conceptualization, Methodology, Writing – original draft, Writing – review & editing, Supervision, Funding acquisition. **Egon Pavlica:** Conceptualization, Methodology, Software, Formal analysis, Data curation, Writing – original draft, Writing – review & editing, Visualization.

Declaration of competing interest

The authors declare that they have no known competing financial interests or personal relationships that could have appeared to influence the work reported in this paper.

Data availability

Data will be made available on request.

Acknowledgments

The work was financially supported by FLAG-ERA JTC 2017 project MX-OSMOPED and by the Slovenian Research Agency ARRS) under research program P1-0055. V. T. and E. T. acknowledge ARRS's support under the Young Researcher's scheme. A.M. acknowledge ARRS's support under research core funding no. P2-0412. N. P. acknowledges ARRS's support under research project no. Z1-3189.

Appendix A. Supplementary data

Supplementary data to this article can be found online at https://doi.org/10.1016/j.diamond.2023.109879.

References

[1] K.S. Novoselov, A.K. Geim, S.V. Morozov, D.-E. Jiang, Y. Zhang, S.V. Dubonos, I. V. Grigorieva, A.A. Firsov, Electric field effect in atomically thin carbon films, Science 306 (5696) (2004) 666–669.
[2] K.I. Bolotin, K.J. Sikes, Z. Jiang, M. Klima, G. Fudenberg, J. Hone, P. Kim, H. Stormer, Ultrahigh electron mobility in suspended graphene, Solid State Commun. 146 (9–10) (2008) 351–355.
[3] X. Li, X. Wang, L. Zhang, S. Lee, H. Dai, Chemically derived, ultrasmooth graphene nanoribbon semiconductors, Science 319 (5867) (2008) 1229–1232.
[4] B. Radisavljevic, A. Radenovic, J. Brivio, V. Giacometti, A. Kis, Single-layer MoS 2 transistors, Nat. Nanotechnol. 6 (3) (2011) 147–150.
[5] Z. Yu, Z.Y. Ong, Y. Pan, Y. Cui, R. Xin, Y. Shi, B. Wang, Y. Wu, T. Chen, Y.W. Zhang, Realization of room-temperature phonon-limited carrier transport in monolayer MoS2 by dielectric and carrier screening, Adv. Mater. 28 (3) (2016) 547–552.
[6] X. Li, J.T. Mullen, Z. Jin, K.M. Borysenko, M.B. Nardelli, K.W. Kim, Intrinsic electrical transport properties of monolayer silicene and MoS 2 from first principles, Phys. Rev. B 87 (11) (2013), 115418.
[7] M. Naguib, M. Kurtoglu, V. Presser, J. Lu, J. Niu, M. Heon, L. Hultman, Y. Gogotsi, M.W. Barsoum, Two-dimensional nanocrystals produced by exfoliation of Ti3AlC2, Adv. Mater. 23 (37) (2011) 4248–4253.
[8] Y. Zhang, C. Ma, W. He, C. Zhang, L. Zhou, G. Wang, W. Wei, MXene and MXene-based materials for lithium-sulfur batteries, Prog. Nat. Sci.: Mater. Int. 31 (4) (2021) 501–513.
[9] Y. Gogotsi, B. Anasori, The Rise of MXenes, ACS Publications, 2019.
[10] S. Ahmad, I. Ashraf, M.A. Mansoor, S. Rizwan, M. Iqbal, An overview of recent advances in the synthesis and applications of the transition metal carbide nanomaterials, Nanomaterials 11 (3) (2021) 776.
[11] H. Shi, P. Zhang, Z. Liu, S. Park, M.R. Lohe, Y. Wu, A. Shaygan Nia, S. Yang, X. Feng, Ambient-stable two-dimensional titanium carbide (MXene) enabled by iodine etching, Angew. Chem. Int. Ed. 60 (16) (2021) 8689–8693.

[12] S. Yang, P. Zhang, F. Wang, A.G. Ricciardulli, M.R. Lohe, P.W. Blom, X. Feng, Fluoride-free synthesis of two-dimensional titanium carbide (MXene) using a binary aqueous system, Angew. Chem. 130 (47) (2018) 15717–15721.
[13] M. Naguib, J. Come, B. Dyatkin, V. Presser, P.-L. Taberna, P. Simon, M. W. Barsoum, Y. Gogotsi, MXene: a promising transition metal carbide anode for lithium-ion batteries, Electrochem. Commun. 16 (1) (2012) 61–64.
[14] Q. Tang, Z. Zhou, P. Shen, Are MXenes promising anode materials for li ion batteries? Computational studies on electronic properties and li storage capability of Ti3C2 and Ti3C2X2 (X= F, OH) monolayer, J. Am. Chem. Soc. 134 (40) (2012) 16909–16916.
[15] O. Mashtalir, M. Naguib, V.N. Mochalin, Y. Dall'Agnese, M. Heon, M.W. Barsoum, Y. Gogotsi, Intercalation and delamination of layered carbides and carbonitrides, Nat. Commun. 4 (1) (2013) 1–7.
[16] M. Naguib, V.N. Mochalin, M.W. Barsoum, Y. Gogotsi, 25th anniversary article: MXenes: a new family of two-dimensional materials, Adv. Mater. 26 (7) (2014) 992–1005.
[17] M. Naguib, O. Mashtalir, J. Carle, V. Presser, J. Lu, L. Hultman, Y. Gogotsi, M. W. Barsoum, Two-dimensional transition metal carbides, ACS Nano 6 (2) (2012) 1322–1331.
[18] A. Enyashin, A. Ivanovskii, Atomic structure, comparative stability and electronic properties of hydroxylated Ti2C and Ti3C2 nanotubes, Comput. Theor. Chem. 989 (2012) 27–32.
[19] Y. Xie, P. Kent, Hybrid density functional study of structural and electronic properties of functionalized ti n+ 1 X n (X= C, N) monolayers, Phys. Rev. B 87 (23) (2013), 235441.
[20] M. Khazaei, M. Arai, T. Sasaki, C.Y. Chung, N.S. Venkataramanan, M. Estili, Y. Sakka, Y. Kawazoe, Novel electronic and magnetic properties of two-dimensional transition metal carbides and nitrides, Adv. Funct. Mater. 23 (17) (2013) 2185–2192.
[21] Y. Lee, S.B. Cho, Y.-C. Chung, Tunable indirect to direct band gap transition of monolayer Sc2CO2 by the strain effect, ACS Appl. Mater. Interfaces 6 (16) (2014) 14724–14728.
[22] M. Khazaei, A. Ranjbar, M. Ghorbani-Asl, M. Arai, T. Sasaki, Y.Y. Liang, S. Yunoki, Nearly free electron states in MXenes, Phys. Rev. B 93 (20) (2016) 10.
[23] W. Zheng, B. Sun, D. Li, S.M. Gali, H. Zhang, S. Fu, L. Di Virgilio, Z. Li, S. Yang, S. Zhou, D. Beljonne, M. Yu, X. Feng, H.I. Wang, M. Bonn, Band transport by large Fröhlich polarons in MXenes, Nat. Phys. 18 (5) (2022) 544–550.
[24] A. Lipatov, A. Goad, M.J. Loes, N.S. Vorobeva, J. Abourahma, Y. Gogotsi, A. Sinitskii, High electrical conductivity and breakdown current density of individual monolayer Ti3C2Tx MXene flakes, Matter 4 (4) (2021) 1413–1427.
[25] S.H. Mir, V.K. Yadav, J.K. Singh, Recent advances in the carrier mobility of two-dimensional materials: a theoretical perspective, ACS Omega 5 (24) (2020) 14203–14211.
[26] G. Bratina, E. Pavlica, Characterisation of charge carrier transport in thin organic semiconductor layers by time-of-flight photocurrent measurements, Org. Electron. 64 (2019) 117–130.
[27] K. Hantanasirisakul, M. Alhabeb, A. Lipatov, K. Maleski, B. Anasori, P. Salles, C. Ieosakulrat, P. Pakawatpanurut, A. Sinitskii, S.J. May, Effects of synthesis and processing on optoelectronic properties of titanium carbonitride MXene, Chem. Mater. 31 (8) (2019) 2941–2951.
[28] H. Ghassemi, W. Harlow, O. Mashtalir, M. Beidaghi, M. Lukatskaya, Y. Gogotsi, M. L. Taheri, In situ environmental transmission electron microscopy study of oxidation of two-dimensional ti 3 C 2 and formation of carbon-supported TiO 2, J. Mater. Chem. A 2 (35) (2014) 14339–14343.
[29] O. Mashtalir, K.M. Cook, V.N. Mochalin, M. Crowe, M.W. Barsoum, Y. Gogotsi, Dye adsorption and decomposition on two-dimensional titanium carbide in aqueous media, J. Mater. Chem. A 2 (35) (2014) 14334–14338.
[30] L. Wang, H. Zhang, B. Wang, C. Shen, C. Zhang, Q. Hu, A. Zhou, B. Liu, Synthesis and electrochemical performance of Ti3C2Tx with hydrothermal process, Electron. Mater. Lett. 12 (5) (2016) 702–710.
[31] A.H. Feng, Y. Yu, Y. Wang, F. Jiang, L. Mi, L.X. Song, Two-dimensional MXene Ti3C2 produced by exfoliation of Ti3AlC2, Mater. Des. 114 (2017) 161–166.
[32] S.R. Pathipati, E. Pavlica, A. Schlierf, M. El Gemayel, P. Samori, V. Palermo, G. Bratina, Graphene-induced enhancement of n-type mobility in perylenediimide thin films, J. Phys. Chem. C 118 (43) (2014) 24819–24826.
[33] G.R. Berdiyorov, Optical properties of functionalized Ti3C2T2 (T = F, O, OH) MXene: first-principles calculations, AIP Adv. 6 (5) (2016).
[34] H. Lashgari, M.R. Abolhassani, A. Boochani, S.M. Elahi, J. Khodadadi, Electronic and optical properties of 2D graphene-like compounds titanium carbides and nitrides: DFT calculations, Solid State Commun. 195 (2014) 61–69.
[35] K. Maleski, C.E. Shuck, A.T. Fafarman, Y. Gogotsi, The broad chromatic range of two-dimensional transition metal carbides, Adv. Opt. Mater. 9 (4) (2020).
[36] D. Zhang, D. Shah, A. Boltasseva, Y. Gogotsi, MXenes for photonics, ACS Photonics 9 (4) (2022) 1108–1116.
[37] K.J. Tielrooij, J.C.W. Song, S.A. Jensen, A. Centeno, A. Pesquera, A. Zurutuza Elorza, M. Bonn, L.S. Levitov, F.H.L. Koppens, Photoexcitation cascade and multiple hot-carrier generation in graphene, Nat. Phys. 9 (4) (2013) 248–252.
[38] H. Lashgari, M. Abolhassani, A. Boochani, S. Elahi, J. Khodadadi, Electronic and optical properties of 2D graphene-like compounds titanium carbides and nitrides: DFT calculations, Solid State Commun. 195 (2014) 61–69.
[39] H. Lin, X. Wang, L. Yu, Y. Chen, J. Shi, Two-dimensional ultrathin MXene ceramic nanosheets for photothermal conversion, Nano Lett. 17 (1) (2017) 384–391.
[40] E. Pavlica, G. Bratina, Time-of-flight mobility of charge carriers in position-dependent electric field between coplanar electrodes, Appl. Phys. Lett. 101 (9) (2012), 093304.
[41] H. Scher, E.W. Montroll, Anomalous transit-time dispersion in amorphous solids, Phys. Rev. B 12 (6) (1975) 2455–2477.
[42] J.C. Scott, L.T. Pautmeier, L.B. Schein, Mean mobilities of charge carriers in disordered media, Phys. Rev. B 46 (13) (1992) 8603–8606.
[43] E. Pavlica, R.B. Penumala, G. Bratina, The role of local potential minima on charge transport in thin organic semiconductor layers, Org. Electron. 42 (2017) 221–227.
[44] K. Hantanasirisakul, M. Alhabeb, A. Lipatov, K. Maleski, B. Anasori, P. Salles, C. Ieosakulrat, P. Pakawatpanurut, A. Sinitskii, S.J. May, Y. Gogotsi, Effects of synthesis and processing on optoelectronic properties of titanium carbonitride MXene, Chem. Mater. 31 (8) (2019) 2941–2951.
[45] D.M. Pai, Transient photoconductivity in poly (N-vinylcarbazole), J. Chem. Phys. 52 (5) (1970) 2285–2291.
[46] J. Frenkel, On pre-breakdown phenomena in insulators and electronic semi-conductors, Phys. Rev. 54 (8) (1938) 647.
[47] R.M. Hill, Poole-frenkel conduction in amorphous solids, Philos. Mag. 23 (181) (1971) 59–86.
[48] L. Pautmeier, R. Richert, H. Bässler, Poole-frenkel behavior of charge transport in organic solids with off-diagonal disorder studied by Monte Carlo simulation, Synth. Met. 37 (1–3) (1990) 271–281.
[49] T. Minari, T. Nemoto, S. Isoda, Temperature and electric-field dependence of the mobility of a single-grain pentacene field-effect transistor, J. Appl. Phys. 99 (3) (2006), 034506.
[50] D.S. Chung, I. Kang, Y.-H. Kim, S.-K. Kwon, Charge transport characteristics of a high-mobility diketopyrrolopyrrole-based polymer, Phys. Chem. Chem. Phys. 15 (35) (2013) 14777–14782.
[51] L. Yu, E. Pavlica, R. Li, Y. Zhong, C. Silva, G. Bratina, C. Müller, A. Amassian, N. Stingelin, Conjugated polymer mesocrystals with structural and optoelectronic coherence and anisotropy in three dimensions, Adv. Mater. 34 (1) (2022), 2103002.
[52] T. Meier, H. Bässler, A. Köhler, The impact of grain boundaries on charge transport in polycrystalline organic field-effect transistors, Adv. Opt. Mater. 9 (14) (2021), 2100115.
[53] N. Karl, Charge carrier transport in organic semiconductors, Synth. Met. 133 (2003) 649–657.
[54] A. Kovtun, A. Candini, A. Vianelli, A. Boschi, S. Dell'Elce, M. Gobbi, K.H. Kim, S. Lara Avila, P. Samorì, M. Affronte, A. Liscio, V. Palermo, Multiscale charge transport in van der waals thin films: reduced graphene oxide as a case study, ACS Nano 15 (2) (2021) 2654–2667.
[55] A.G. Kelly, T. Hallam, C. Backes, A. Harvey, A.S. Esmaeily, I. Godwin, J. Coelho, V. Nicolosi, J. Lauth, A. Kulkarni, All-printed thin-film transistors from networks of liquid-exfoliated nanosheets, Science 356 (6333) (2017) 69–73.
[56] A.G. Kelly, D. O'Suilleabhain, C. Gabbett, J.N. Coleman, The electrical conductivity of solution-processed nanosheet networks, Nat. Rev. Mater. (2021) 1–18.
[57] K. Hantanasirisakul, Y. Gogotsi, Electronic and optical properties of 2D transition metal carbides and nitrides (MXenes), Adv. Mater. 30 (52) (2018), 1804779.
[58] A.D. Dillon, M.J. Ghidiu, A.L. Krick, J. Griggs, S.J. May, Y. Gogotsi, M.W. Barsoum, A.T. Fafarman, Highly conductive optical quality solution-processed films of 2D titanium carbide, Adv. Funct. Mater. 26 (23) (2016) 4162–4168.
[59] G. Li, K. Kushnir, Y. Dong, S. Chertopalov, A.M. Rao, V.N. Mochalin, R. Podila, L. V. Titova, Equilibrium and non-equilibrium free carrier dynamics in 2D Ti3C2Tx MXenes: THz spectroscopy study, 2D Mater. 5 (3) (2018) 035043.